Deletion of the transmembrane protein Prom1b in zebrafish disrupts outer-segment morphogenesis and causes photoreceptor degeneration

Lu, Zhaojing; Hu, Xuebin; Reilly, James; Jia, Danna; Liu, Fei; Yu, Shanshan ; Liu, Xiliang; Xie, Shanglun; Qu, Zhen; Qin, Yayun ; Huang, Yuwen; Lv, Yuexia; Li, Jingzhen; Gao, Pan; Wong, Fulton; Shu, Xinhua; Tang, Zhaohui; Liu, Mugen

Published in:
Journal of Biological Chemistry

DOI:
10.1074/jbc.RA119.008618

Publication date:
2019

Document Version
Author accepted manuscript

Deletion of the transmembrane protein Prom1b in zebrafish disrupts outer-segment morphogenesis and causes photoreceptor degeneration

Zhaojing Lu[1,+] , Xuebin Hu[1,2,+] , James Reilly[3] , Danna Jia[1] , Fei Liu[1] , Shanshan Yu[1] , Xiliang Liu[1] , Shanglun Xie[1] , Zhen Qu[1] , Yayun Qin[1] , Yuwen Huang[1] , Yuexia Lv[1] , Jingzhen Li[1] , Pan Gao[1] , Fulton Wong[4] , Xinhua Shu[3] , Zhaohui Tang[1]*, Mugen Liu[1]*

1 Key Laboratory of Molecular Biophysics of Ministry of Education, College of Life Science and Technology, Huazhong University of Science and Technology, Wuhan, Hubei 430074, P.R. China

2 State Key Laboratory of Ophthalmology, Zhongshan Ophthalmic Center, Sun Yat-sen University, Guangzhou, Guangdong 510060, P.R. China;

3 Department of Life Sciences, Glasgow Caledonian University, Glasgow G4 0BA, UK

4 Department of Ophthalmology, Duke University School of Medicine, Durham, NC 27710, USA

Running title: Prom1b deletion causes photoreceptor degeneration +These authors contributed equally to this work.

*To whom correspondence should be addressed at: Key Laboratory of Molecular Biophysics of Ministry of Education, College of Life Science and Technology, Huazhong University of Science and Technology, 1037 Luoyu Road, Wuhan, P. R. China. Tel: +86 27 87794549; Fax: +86 27 87794549; Email: lium@hust.edu.cn (M.L.); zh_tang@mail.hust.edu.cn (Z.T.)

Abstract

Mutations in human prominin 1 (PROM1), encoding a transmembrane glycoprotein localized mainly to plasma membrane protrusions, have been reported to cause retinitis pigmentosa, macular degeneration and cone-rod dystrophy. Although the structural role of PROM1 in outersegment (OS) morphogenesis has been demonstrated in Prom1-knockout mouse, the mechanisms underlying these complex disease phenotypes remain unclear. Here we utilized a zebrafish model to further investigate PROM1's role in the retina. The Prom1 orthologs in zebrafish include prom1a and prom1b, and our results showed that prom1b, rather than prom1a, plays an important role in zebrafish photoreceptors. Loss of prom1b disrupted OS morphogenesis, with rods and cones exhibiting differences in impairment: cones degenerated at an early age, whereas rods remained viable, but with an abnormal OS, even at 9 months post-fertilization. Immunofluorescence experiments with WT zebrafish revealed that Prph2, an ortholog of the human transmembrane protein peripherin 2 and also associated with OS formation, is localized to the edge of OS and is more highly expressed in the cone OS than in the rod OS. Moreover, we found that Prom1b deletioncauses mislocalization of Prph2 and disrupts its oligomerization. We conclude that the variation in Prph2 levels between cones and rods was one of the reasons for the different PROM1 mutationinduced phenotypes of these retinal structures. These findings expand our understanding of the phenotypes caused by PROM1 mutations and provide critical insights into its function.

Keywords: retinal degeneration, prominin 1 (PROM1), photoreceptor, morphogenesis, peripherin 2 (PRPH2), eye disease, *Danio rerio*

Human PROM1 (also known as CD133, RP41, MCDR2, STGD4 and CORD12) encodes a 5-transmembrane glycoprotein localized mainly to plasma membrane protrusions (1). It was identified originally as a surface antigen in the hematopoietic stem and progenitor cells (2) and later detected also in various differentiated epithelial and nonepithelial cells (3-6). Although PROM1 is expressed in various tissues throughout embryogenesis and adulthood, mutations in the PROM1 gene cause mainly retinal diseases. Human PROM1 gene mutations lead to extremely variable retinal clinical phenotypes, including cone photoreceptor- or macular-dominated disorders such as macular degeneration (MD), autosomal dominant Stargardt-like macular dystrophy (7), autosomal dominant bull's-eye macular dystrophy (7), autosomal dominant conerod dystrophy (CRD) (7,8), autosomal recessive CRD (8-15), and the rod photoreceptor-dominated disorder autosomal recessive retinitis pigmentosa (RP) (6,16-20). So far, 24 PROM1 mutations, predominantly truncation mutations along with some missense mutations, have been reported: 22 of them are associated with an autosomal recessive mode of inheritance while 16 of them have been identified in patients with CRD. The mechanisms underlying this phenotypic heterogeneity are largely unknown.

Vertebrate photoreceptors are neural cells specialized in light detection. The phototransduction apparatus is housed in a cellular compartment known as the outer-segment (OS). The OS, which contains a stack of membranous disks, is renewed daily by the formation of new disks at its base and the shedding of older disks from its distal tip. The shed disks are phagocytosed by retinal pigment epithelium (RPE) cells. Several studies have shown that mouse PROM1 is localized to the base of the photoreceptor OS where the new disks membranes are formed (1,7), whereas, in Xenopus, Prom1 is distributed to the outer rims of open disk lamellae of cone OSs and basal disks of rod OSs (21). In human and murine retinas, the PROM1 protein is purported to have a crucial role in the formation of the OS. Deletion of PROM1 in mouse resulted in abnormal photoreceptor OS morphogenesis of both rods and cones. However, the function of PROM1 in photoreceptor OS formation is still unclear.

PROM1 is evolutionarily conserved from C. elegans to Drosophila, zebrafish, Xenopus, mouse and human. Zebrafish prom1 orthologues include prom1a and prom1b (22). In the present study, we constructed prom1a and prom1b knockout zebrafish lines. Our results show that prom1a deletion in zebrafish has no deleterious effect on photoreceptors. On the other hand, prom1b knockout zebrafish show serious retinal degeneration at an early age. It is notable that cones and rods are affected differently although the primary defect in both photoreceptor subtypes is disruption of disk morphogenesis. Cones degenerate with the onset of OS formation, while the rods are still present at 9 months post fertilization (mpf), although with partly disorganized and longer OSs.

Another gene that is known to be involved in OS formation is PRPH2 (also known as retinal degeneration slow, RDS). This protein forms oligomers and localizes to the rim of OS. Like PROM1, mutations in PRPH2 also cause phenotypic heterogeneity, resulting in RP, CRD or MD (23-25). Here we report that deletion of Prom1b causes mislocalization and disrupts oligomerization of Prph2. Additionally, our immunofluorescence results indicate that cones possess a higher protein content of Prph2 than rods, which may be one of the reasons for the different phenotypes in rods and cones in prom1b-/- zebrafish. Accordingly, our results provide mechanistic insights into the function of Prom1b and the nature of the phenotype caused by its deletion.

Results

Generation of prom1a-/- and prom1b-/- zebrafish lines

In this study, we constructed prom1a and prom1b knockout zebrafish lines by the transcription activator-like effector nucleases (TALENs) technology. Both of their TALENs binding sites were separated by a 16-bp DNA spacer (Fig. 1, A and B). By mutant screening over three generations of zebrafish, we selected prom1a mutation (prom1a$^{-/-}$) (c.138_141delTACT, p.Asp46Glu fs*15) and prom1b mutation (prom1b- /-) (c.174_177delACCA, p.Pro59Val fs*62) zebrafish lines for subsequent experiments; the genomic DNA sequencing results are shown in Fig. 1, C and D. Additionally, we detected the Prom1b protein expression by Western blot (antibody against Prom1b was prepared by Dia-An, Inc, in Wuhan, China), and the result confirmed that no Prom1b protein existed in the mutant zebrafish, which further demonstrated the successful construction of the prom1b$^{-/-}$ zebrafish line (Fig. 1G). Unfortunately, we failed to generate a usable antibody against Prom1a. Compared with wildtype (WT) zebrafish, the mRNA expression levels of prom1a showed no significant change at 2mpf, while that of prom1b exhibited a decrease at 7 days post fertilization (dpf) (Fig. 1, E and F). The mutated cDNA sequences of prom1a and prom1b, including a section of the region encompassing exon 1 and exon 2, are shown in Supplementary Fig. S1, a finding that could also indicate the knockout design was effective.

Prom1b$^{-/-}$ zebrafish displayed retinal degeneration phenotypes

To assess the effects of prom1a and prom1b knockout on the zebrafish retina, we first examined their retinal morphology. Retinal sections were obtained at the age of 1mpf and stained with hematoxylin/eosin (HE). The results showed that there was no obvious difference in cell layer organization between the mutant and WT zebrafish. However, cells in the outer nuclear layer (ONL) of prom1b-/- zebrafish were sparsely distributed, compared with WT zebrafish (Fig. 2A). Furthermore, an increased level of apoptotic cells (about 3-fold) was clearly observed in the prom1b-/- compared to WT zebrafish at 1mpf (Fig. 2, B and C). The thickness of the ONL and OSs in prom1a-/- was similar to those in WT zebrafish even at 11mpf (Supplementary Fig. S2), which suggested that knockout of prom1a in zebrafish might cause no impairment to photoreceptors. To investigate the reason for the different phenotypes of prom1a- /- and prom1b-/- zebrafish, we generated GFPhPROM1, GFP-zfProm1a and GFP-zfProm1b and expressed the plasmids in ARPE-19 cells. We observed that zfProm1b was mainly localized on the protuberances of the cell membrane, which was similar with hPROM1, while zfProm1a was localized in the cytoplasm. We also observed a similar distribution of zfProm1b and hPROM1 using HeLa cells (Supplementary Fig. S3). These results indicated that the function of Prom1a is different from hPROM1 in photoreceptors.

Additionally, we examined the expression of some proteins involved in the phototransduction cascade, including rod-special proteins (GNB1, GNAT1) and cone-special proteins (GNB3, GNAT2) (26). These proteins are essential for converting light signals into electrical signals, and any impairment would affect normal visual function. Results from Western blot showed a significant decrease in expression of Gnb3 and Gnat2 in the prom1b-/- compared to WT zebrafish at 1mpf and 3mpf, while an increased expression of Gnb1 and Gnat1 was observed at the same ages (Fig. 3, A, B and C). However, there was no significant differences in the expression of the four proteins between prom1a-/- and WT zebrafish even at 11mpf (Fig. 3, A and D).

The results obtained above indicate that prom1b, rather than prom1a, plays an important role in zebrafish photoreceptors, and that loss of Prom1b in zebrafish would lead to severe retinal

degeneration phenotypes. Therefore, in the subsequent research we mainly study the pathogenic mechanism of retinal degeneration caused by PROM1 mutation in the prom1b-/- zebrafish line.

Prom1b deletion in zebrafish caused different impairments to different photoreceptors

As obvious characteristics of retinal degeneration were observed in the prom1b-/- zebrafish retina, we wanted to further explore possible differences in different photoreceptors. With the exception of their UV (ultra-violet) cones, zebrafish possess similar photoreceptor types to human. We labelled rods and cones (red, green, blue and UV cones) with specific antibodies respectively (rhodopsin, opn1lw, opn1mw, opn1sw2 and opn1sw1) in retinal sections for WT and prom1b-/- zebrafish, at different ages. Our results showed that the OSs of all five types of photoreceptor exhibited a neat and compact arrangement in the WT zebrafish, but that prom1b- /- zebrafish OSs displayed different impairments with respect to number and morphology (Fig. 4, A and B). The number of red and green cone OSs in prom1b-/- zebrafish decreased from the age of 7dpf, and with time this decrease became more obvious (Fig. 5, A and B); compared with the WT zebrafish the number of blue and UV cone OSs showed only a slight decrease at 7dpf, but had decreased noticeably at 1mpf, with only a few OSs remaining by 3mpf (Fig. 5, C and D; Supplementary Fig. S4 and S5); the number of rod OSs in prom1b-/- zebrafish showed no difference from the WT zebrafish at 7dpf; however, the length of rod OSs showed a clear increase at 1mpf, while rods still existed even at 9mpf (Fig. 5E; Supplementary Fig. S6). In short, our results indicate that Prom1b deletion in zebrafish had different effects on cones and rods: the number of cones was reduced, while the length of rod OSs became longer.

Outer-segment morphogenesis was disrupted in prom1b$^{-/-}$ zebrafish

Next, we carried out a transmission electron microscopy (TEM) assay to assess ultrastructural changes of the photoreceptors in prom1b-/- zebrafish. At 3dpf, the normal stacked disk morphology of photoreceptor OSs could be clearly observed in WT zebrafish; by contrast there were few, or occasionally several, quite small whorl-like disk structures detected in prom1b-/- zebrafish at the same age (Fig. 6A). Additionally, we analyzed the levels of apoptosis by TUNEL (TdT-mediated dUTP nick end labelling) staining at 3dpf: the results showed no differences in cell death in the ONL of prom1b-/- compared to WT zebrafish (Fig. 6B). According to previous research, zebrafish OSs appear during 55-63 hours post-fertilization (hpf) (27-30); our observations suggest that Prom1b deletion would delay the development of OSs.

Subsequently, we continued to examine the ultrastructural changes of the photoreceptor OSs at different ages. Examination by TEM revealed that the disk structures of OS already existed at 10dpf, but that these disks were highly disorganized in prom1b-/- zebrafish (Fig. 7, A-C). Interestingly, we found that these abnormal disks exhibited different morphological characteristics, which have not been described before in any Prom1-deficient mouse models (1,7). In particular, some of the disks were completely curved around into whorllike structures (Fig. 7E); some of the disks were overgrown and misoriented at the distal end of the OS (Fig. 7F); some of the disks were overgrown at the base of the OS, while the morphology of the entire OS was abnormal compared with WT zebrafish (Fig. 7, D and G); some of the disks were neatly stacked and elongated at both the base and distal end of the OS, while part of these disks at the middle of the OS exhibited misorientation (Fig. 7H). By 2mpf, there was some photoreceptor degeneration, in the prom1b-/- zebrafish, although some photoreceptors still existed (Fig. 7I). Combining the results of our immunofluorescence (IF)

studies, we concluded that the photoreceptors that had been retained were mainly rods. From one of the enlarged figures, it can be seen that the disks of rod OSs were mild disorganized, while overgrowth of disks still appeared (Fig. 7, J, a and b). In addition, we observed that some shed disks were accumulated in the apical region of OSs. (Fig. 7I; Supplementary Fig. S7) Together, these results show that both rods and cones disk membranes were disorganized in prom1b-/- zebrafish, but that cones were impaired more acutely than rods. Prom1b deletion affects

Prph2 protein distribution and oligomerization

PRPH2 is a key structural protein of the OS. It is localized to the disk rim of the rods and cones and is necessary for the formation of the OS (23,31). Prph2-/- mice failed to develop OS structures, while the Prph2+/- mice formed disorganized OSs with whorl-like structures (32,33). It is notable that PRPH2 mutations in human manifest as rod and/or cone dystrophies with varying levels of severity (34), and that previous studies have demonstrated the distinct functions of PRPH2 in rods and cones (35-37). In our current studies, Prom1b deletion in zebrafish exerted different effects on the disk formation of rod and cone OSs, with the pattern of disks being similar to that seen in $Prph2^{+/-}$ mice, all of which led us to consider whether there was a relationship between prom1b and prph2. Therefore, we focused on the Prph2 protein in the subsequent research.

In order to examine the cellular localization of Prph2, we labelled photoreceptors with specific antibodies (Prph2, Rhodopsin, Opn1lw) in retinal sections from WT and prom1b-/- zebrafish at 2mpf (rods and a few red cones were still present in the retina at this period). In the WT zebrafish, Prph2 was mainly localized to the edge (most likely the disk rim) of the rod and cone OSs (Fig. 8, A–F, af), with signal intensity in cone OSs being stronger than that in rod OSs (Supplementary Fig. S8), indicating a higher protein content of Prph2 in cone OSs. In the $prom1b^{-/-}$ zebrafish, we found Prph2 signals almost completely filling the red cone OS rather than just on its edge (Fig. 8, J-L, jl), while occasionally mislocalization of Prph2 appeared in the partial OSs of rods (Fig. 8, G-I, gi). Moreover, we also found mislocalization of Prph2 in the OSs of $prom1b^{-/-}$ zebrafish at an early age (14dpf, Supplementary Fig. S9).

In photoreceptor OSs, Prph2 forms higherorder oligomers, which localize to the disk rim and play a crucial role in disk rim formation (24). A number of previous studies have confirmed that oligomerization of Prph2 is essential for OS formation (24,38). Since mislocalization of Prhp2 and malformation of OSs were observed in the current study, we asked whether the Prom1b deletion would affect the oligomerization of Prph2. By non-reducing Western blot analysis, we found that the ratio of Prph2 dimer to monomer was reduced in zebrafish at an earlier age (7dpf) (Fig. 9, A and a). These results further demonstrated that the localization of Prph2 in the disk was affected in the mutant zebrafish. Furthermore, to evaluate the influence on protein levels of Prph2, Western blot analysis was performed on retinal extracts from WT and $prom1b^{-/-}$ zebrafish at different ages. The results showed that the protein expression of Prph2 also significantly decreased at 7dpf and 2mpf (Fig. 9, B and b). In addition, we found that the mRNA expression of prph2 (there are two isoforms, prph2a and prph2b, in zebrafish) also decreased in $prom1b^{-/-}$ zebrafish at the same period (Fig. 9, C and D). Based on the fact that photoreceptor number reduced at an early age, the decreased level of Prph2 likely resulted from a consequence of the OS phenotypes following Prom1b deletion.

Discussion

PROM1 mutations lead to more complex clinical phenotypes of retinal degeneration. Patients with mutations in PROM1 were initially diagnosed as having autosomal-recessive retinal degeneration. The affected individuals reported night blindness and loss of peripheral vision from childhood with progression to profound visual impairment and extinguished electroretinograms by their third decade (6). Subsequently, a homozygous mutation resulting in a truncated PROM1 protein was identified in a family with severe RP, the affected patients reporting night blindness and decreased visual acuity in early childhood, with all of them having typical and advanced RP fundus changes accompanied by macular changes (20). Recently, many mutations of PROM1 have been implicated in patients with CRD: these patients had central visual dysfunction from early childhood, manifesting as nystagmus, mild photophobia and color vision deficiency, while night vision deteriorated in adolescence (11,12,19). Additionally, there is another autosomal-dominant mutation, PROM1/R373C, that results in stable mutant protein and interferes with the action of the normal protein, causing Stargardt-like MD, bull's-eye MD and CRD (7). Due to complex and variable clinical phenotypes caused by PROM1 mutations, it is not possible to use one animal model to reflect all clinical phenotypes. In this study, we generated a new PROM1 knockout animal model to provide a new perspective for research into the function of PROM1. The major findings of this study are the following: (1) Prom1b, rather than Prom1a, plays an important role in the zebrafish photoreceptors; (2) Prom1b deletion disrupts OS morphogenesis and causes photoreceptor degeneration, but that the effect on cones is more acute than in rods; (3) mislocalization of Prph2 and decreased ratio of Prph2 dimer to monomer are part of the mechanisms for the phenotypes caused by Prom1b deletion.

The retinal phenotype of prom1b-knockout zebrafish is not identical to the Prom1-knockout mouse. In both animal models, photoreceptors degenerate at an early age and the disks are disorganized. However, there are still clear differences. In Prom1-knockout mouse, both rod and cone disks appear overgrown and misoriented throughout the entire OS, and degenerate at a same time. In prom1b-/- zebrafish, cone disks exhibit serious disorganization while rod OSs exhibit only mild misorientation; cones degenerated at an early age while rods were alive, albeit with abnormal OS, even at 9mpf (1). We speculate that the distinct phenotypes between mouse and zebrafish models may be caused by the different photoreceptor structure and by a different distribution of PROM1. In some species the OSs of the photoreceptors are surrounded by structures called calyceal processes, which are composed of actin filaments and which play a supporting role for OS structure. Calyceal processes surround the proximal outer-segment in rods, and are paraxially aligned with the outersegment in cones (39,40). These calyceal processes exist in humans, rhesus monkey and zebrafish, but not in mouse (41). PROM1 might have an essential role in maintaining the calyceal processes through two of its interaction proteins: actin and EYS. Due to the function of PROM1 in calyceal processes, deletion of Prom1b in zebrafish might have different effects on rods and cones. In humans, the PROM1 protein has been reported to be distributed throughout the entire cone OS and the basal disk of the rod OS (42). A similar distribution of Prom1 has been observed in Xenopus laevis, while in the mouse Prom1 is localized exclusively to the base disk of both rods and cones. Based on the phenotype of prom1b-/- zebrafish, we speculate that the zebrafish is likely to have a Prom1 distribution similar to that of Xenopus laevis and human. However, we failed to confirm this speculation as our antibody against zebrafish Prom1b didn't work in IF analysis.

PRPH2 is another crucial protein for disk morphogenesis. Mutations that affected PRPH2 oligomerization caused more severe defects in cones than in rods (24). In our study, we detected

that Prph2 signal intensity in cones was notably stronger than that in rods, which is an important finding, indicating that cones and rods possess different Prph2 protein levels. We consider this different protein content of Prhp2 as being one of the reasons for the different phenotypes of cones and rods. Furthermore, our results showed that loss of Prom1b disrupted oligomerization and caused mislocalization of Prph2. Han et al. (21) report that Prom1 and Prph2 are mutually exclusively distributed in X. laevis cone OSs, and suggest the two proteins must be tightly coordinated (possibly through a counterbalance relationship) to mediate the disk morphogenesis. Here, we detected that there is no direct protein interaction between Prom1b and Prph2, which suggests that the relationship between the two proteins in zebrafish may be similar to that in X. laevis. Interestingly, our results show that Prph2 does not localize specifically to the disk rims, as it also appeared to localize to disk membranes in prom1b-/- zebrafish. Another independent study by Conley et al. (43) show that Prph2 deletion in amphibian leads to Prom1 localization in both disk rim and membrane, but does not affect distribution of other disk membrane-specific proteins (such as S-opsin). Conley et al. (43) and our experimental results together support the suggestion provided by Han et al (21). Therefore, we consider that the abnormal distribution of Prph2 in prom1b-/- zebrafish may result from disruption of a counterbalance relationship between Prom1 and Prph2. Moreover, we found that the ratio of Prph2 dimer to monomer was significantly reduced following Prom1b deletion. We are not clear what caused the ratio to decrease, but we speculate that this is associated with the mislocalized Prhp2. Given that impairment of Prph2 oligomerization would affect disk formation, the changes in the Prph2 oligomer and distribution are likely to be part of the mechanism for OS defects in prom1b-/- zebrafish. Our findings provide critical clues for understanding the relationship between PROM1 and PRPH2 in the disk formation.

However, it is still difficult to account for the fact that rod OS length becomes longer in prom1b-zebrafish. Typically, disks in rods are detached from the plasma membrane while cone disks are continuous with the membrane; it could be that loss of Prom1b may affect structures or mechanisms that are responsible for shedding of the distal rod OS, thus accounting for the longer OS. A recent study showed that PROM1 is a regulator of autophagy in the human retinal pigment epithelium (RPE) (44). Autophagy is important to the health and function of the RPE and retina (45) and alterations in autophagy flux have been reported in some retinal degeneration diseases like MD and RP (46-48). The effects of Prom1b deletion on retinal autophagy activity and its relationship with photoreceptor degeneration require further study in order to elucidate the precise role of PROM1.

In summary, we generated a new PROM1 knockout animal model in this study. Using the prom1b-/- zebrafish, we found that loss of Prom1b caused more severe impairments in cone photoreceptors, and that Prom1b plays a vital role in regulating the distribution of Prph2 in disks. These findings contribute to the understanding of PROM1-related retinal degeneration diseases, and provide key clues for further understanding of the molecular function of PROM1.

Experimental procedures

Zebrafish maintenance

Zebrafish larvae and adults were maintained at 26-28.5℃ under a 14/10 hour light/dark cycle. Fertilized eggs were collected and maintained in E3 medium in an incubator (at ~28.5℃) for 72 hours until the larvae hatched (49). All procedures involving zebrafish were approved by the Ethics

Committee of Huazhong University of Science and Technology and were in accordance with the ARRIVE guidelines.

Cell culture and transfection

Cells were cultured in DMEM medium (HLEC and HeLa) or DMEM/F12 medium (ARPE-19) containing 10% fetal bovine serum and incubated at 37°C in 5% CO2 in a humidified incubator. When grown to 80-90% confluence, cells were replated at a split ratio of 1:3-1:5. Cell transfection was performed with Lipofectamine™ 3000 (Invitrogen).

Antibodies

The list of antibodies used in the present study is provided in Supplementary Table S1.

Generation of prom1a$^{-/-}$ and prom1b$^{-/-}$ zebrafish lines

Both prom1a$^{-/-}$ and prom1b$^{-/-}$ zebrafish lines were constructed utilizing the Golden Gate TALEN kit, as previously described (50). Primers used to amplify the DNA fragment containing the prom1a and prom1b target site are listed below: prom1a, Forward (5' to 3'): CCGGACAGCAGGACTTGAGACC Reverse (3' to 5'): GGGCTGAACCACAAAGAGGAAAG prom1b, Forward (5' to 3'): TCCGTCCTCCCCTTTTTTCCCTA Reverse (3' to 5'): TGGGGAAGGGGTTTGGCTGAA

Hematoxylin-Eosin staining

Zebrafish eyes were isolated and fixed with 4% paraformaldehyde in PBS for 12h at 4 ℃, cryoprotected in 30% sucrose overnight, and embedded in OCT compound. Cryostat sections (10-15μm thick) containing the whole retina including the optic disk were stained with hematoxylin and eosin. For each section, digitized images of the retina were captured using a commercial imaging system.

Transmission electron microscopy

Zebrafish eyes were isolated and left in the fixative (2.5% glutaraldehyde in 0.1M PBS buffer, pH 7.4) overnight at 4℃. After three washes with PBS, the eyes were fixed in 1% osmium tetroxide for 2 hours at room temperature then dehydrated through an ethanol gradient followed by treatment with propylene oxide and embedded in epoxy medium. Ultrathin sections of 100nm thickness were prepared using an ultramicrotome and stained for transmission electron microscopy (TEM).

Immunocytochemistry

Transfected cells were fixed in PBS/10% formaldehyde for 10min, permeabilized with PBS/0.5% Triton X-100 for 15 min and blocked with PBS/10% normal goat serum for 1 h at room temperature (RT). Cells were then incubated with the primary antibody (1:500–1000) soluble in PBS/1% BSA at 4°C overnight and Alexa Fluor 488 nm or 594 nm secondary antibody (1:1000; Molecular Probes®) for 1 h at 37°C. After staining with DAPI for 5 min, slides were mounted. Fluorescence images were captured using a confocal laser-scanning microscope (Fluo ViewtM FV1000 confocal microscope, Olympus Imaging).

Immunohistochemistry and histology

Zebrafish eyes were isolated and fixed with 4% paraformaldehyde in PBS for 12 h at 4 °C, cryoprotected in 30% sucrose overnight, and embedded in OCT compound. Cryostat sections (10–15 μm thick) containing the whole retina including the optic disk were rinsed with PDT (PBS solution containing 1% DMSO and 0.1% Triton X-100) for 10 min and blocked with blocking solution (PDT containing 1% BSA and 10% normal goat serum) for 1 h at RT. Primary antibodies (1:500–1000) were prepared in blocking solution containing 2% normal goat serum and slides were incubated overnight at 4 °C. Slides were washed 3 times with PDT and incubated with Alexa Fluor 488 nm or 594 nm secondary antibody (1:1000; Molecular Probes®) for 1 h at 37 °C. DAPI was diluted with PBS to final 5 μg/mL and used to label the nucleus. The slides were washed 3 times with PBS and then mounted under glass coverslips. Fluorescence images were captured using a confocal laserscanning microscope (Fluo ViewtM FV1000 confocal microscope, Olympus Imaging).

TUNEL staining

TUNEL staining was performed using the TUNEL BrightRed Apoptosis Detection Kit (Vazyme Biotech) according to the manufacturer's instructions. Generally, cryosections were airdried at RT, fixed with 4% paraformaldehyde in PBS for 30 minutes. The slides were washed 2 times with PBS for 15 minutes and incubated with proteinase K buffer for 10 minutes. After that, slides were washed 2-3 times with PBS and incubated with equilibration buffer for 10-30 minutes. The retinal sections were then incubated in TdT buffer at 4℃ overnight. The next day, after DAPI label, the slides were mounted under glass coverslips.

RNA extraction and RT-qPCR

Total RNA of zebrafish was extracted using Trizol (Takara), and quantitated by NanoDrop spectrometry (Thermo Scientific, Wilmington, DE, USA). cDNA was generated by MMLV reverse transcriptase (Invitrogen). Real-time PCR was performed using AceQ® qPCR SYBR® Green Master Mix (Vazyme) according to the manufacturer's instructions and relative gene expression was quantified using the StepOnePlusTM Real-Time PCR System (Life Technologies). Gene primers are listed in Supplementary Table S2.

Western blot

Cells and zebrafish eyes were collected and lysed in SDS lysis buffer with protease inhibitor cocktail. Protein concentration was determined using the BCA protein assay kit (Beyotime, China). Proteins were separated by 12% SDS-PAGE and transferred to nitrocellulose membranes (Millipore). The blots were incubated with primary antibodies (1:500–5000), followed by HRP-labeled secondary antibodies (1: 20,000, Thermo). Super Signal ECL substrate (Pierce) was used for the detection of signals.

Plasmid constructs

The full-length PROM1, Prom1a and Prom1b cDNAs were subcloned into the pEGFP-N1 and pCDNA3.1 vectors.

Statistical analysis

All data are presented as mean ± SD. Data groups were compared by Student's t-test (Prism 6.0 software; Graphpad Software, Inc., La Jolla, CA, USA). Differences between groups were considered statistically significant if $P<0.05$.

Conflict of interest

The authors declare that they have no conflicts of interest with the contents of this article.

References

1. Zacchigna, S., Oh, H., Wilsch-Brauninger, M., Missol-Kolka, E., Jaszai, J., Jansen, S., Tanimoto, N., Tonagel, F., Seeliger, M., Huttner, W. B., Corbeil, D., Dewerchin, M., Vinckier, S., Moons, L., and Carmeliet, P. (2009) Loss of the cholesterol-binding protein prominin-1/CD133 causes disk dysmorphogenesis and photoreceptor degeneration. J. Neurosci. 29, 2297-2308

2. Miraglia, S., Godfrey, W., Yin, A. H., Atkins, K., Warnke, R., Holden, J. T., Bray, R. A., Waller, E. K., and Buck, D. W. (1997) A novel five-transmembrane hematopoietic stem cell antigen: isolation, characterization, and molecular cloning. Blood. 90, 5013-5021

3. Fargeas, C. A., Joester, A., Missol-Kolka, E., Hellwig, A., Huttner, W. B., and Corbeil, D. (2004) Identification of novel prominin-1/CD133 splice variants with alternative C-termini and their expression in epididymis and testis. J. Cell. Sci. 117, 4301-4311

4. Immervoll, H., Hoem, D., Sakariassen, P. O., Steffensen, O. J., and Molven, A. (2008) Expression of the "stem cell marker" CD133 in pancreas and pancreatic ductal adenocarcinomas. BMC. Cancer. 8, 48

5. Horst, D., Kriegl, L., Engel, J., Kirchner, T., and Jung, A. (2008) CD133 expression is an independent prognostic marker for low survival in colorectal cancer. Brit. J. Cancer. 99, 1285-1289

6. Maw, M. A., Corbeil, D., Koch, J., Hellwig, A., Wilson-Wheeler, J. C., Bridges, R. J., Kumaramanickavel, G., John, S., Nancarrow, D., Roper, K., Weigmann, A., Huttner, W. B., and Denton, M. J. (2000) A frameshift mutation in prominin (mouse)-like 1 causes human retinal degeneration. Hum. Mol. Genet. 9, 27-34

7. Yang, Z. L., Chen, Y. L., Lillo, C., Chien, J., Yu, Z. Y., Michaelides, M., Klein, M., Howes, K. A., Li, Y., Kaminoh, Y., Chen, H. Y., Zhao, C., Chen, Y. H., Al-Sheikh, Y. T., Karan, G., Corbeil, D., Escher, P., Kamaya, S., Li, C. M., Johnson, S., Frederick, J. M., Zhao, Y., Wang, C. G., Cameron, D. J., Huttner, W. B., Schorderet, D. F., Munier, F. L., Moore, A. T., Birch, D. G., Baehr, W., Hunt, D. M., Williams, D. S., and Zhang, K. (2008) Mutant prominin 1 found in patients with macular degeneration disrupts photoreceptor disk morphogenesis in mice. J. Clin. Invest. 118, 2908-2916

8. Boulanger-Scemama, E., El Shamieh, S., Demontant, V., Condroyer, C., Antonio, A., Michiels, C., Boyard, F., Saraiva, J. P., Letexier, M., Souied, E., Mohand-Said, S., Sahel, J. A., Zeitz, C., and Audo, I. (2015) Next-generation sequencing applied to a large French cone and cone-rod dystrophy cohort: mutation spectrum and new genotype-phenotype correlation. Orphanet. J. Rare. Dis. 10, 85

9. Mayer, A. K., Rohrschneider, K., Strom, T. M., Glockle, N., Kohl, S., Wissinger, B., and Weisschuh, N. (2016) Homozygosity mapping and whole-genome sequencing reveals a deep intronic PROM1 mutation causing cone-rod dystrophy by pseudoexon activation. Eur. J. Hum. Genet. 24, 459-462

10. Zhang, X., Ge, X. L., Shi, W., Huang, P., Min, Q. J., Li, M. H., Yu, X. P., Wu, Y. M., Zhao, G. Y., Tong, Y., Jin, Z. B., Qu, J., and Gu, F. (2014) Molecular Diagnosis of Putative Stargardt Disease by Capture Next Generation Sequencing. PLoS. One. 9, e95528

11. Khan, A. O., and Bolz, H. J. (2015) Pediatric Cone-Rod Dystrophy with High Myopia and Nystagmus Suggests Recessive PROM1 Mutations. Ophthalmic. Genetics. 36, 349-352

12. Pras, E., Abu, A., Rotenstreich, Y., Avni, I., Reish, O., Morad, Y., Reznik-Wolf, H., and Pras, E. (2009) Cone-rod dystrophy and a frameshift mutation in the PROM1 gene. Mol. Vis. 15, 1709-1716

13. Beryozkin, A., Zelinger, L., Bandah-Rozenfeld, D., Shevach, E., Harel, A., Storm, T., Sagi, M., Eli, D., Merin, S., Banin, E., and Sharon, D. (2014) Identification of Mutations Causing Inherited Retinal Degenerations in the Israeli and Palestinian Populations Using Homozygosity Mapping. Invest. Ophth. Vis. Sci. 55, 1149-1160

14. Littink, K. W., Koenekoop, R. K., van den Born, L. I., Collin, R. W. J., Moruz, L., Veltman, J. A., Roosing, S., Zonneveld, M. N., Omar, A., Darvish, M., Lopez, I., Kroes, H. Y., van Genderen, M. M., Hoyng, C. B., Rohrschneider, K., van Schooneveld, M. J., Cremers, F. P. M., and den Hollander, A. I. (2010) Homozygosity Mapping in Patients with Cone-Rod Dystrophy: Novel Mutations and Clinical Characterizations. Invest. Ophth. Vis. Sci. 51, 5943-5951

15. Eidinger, O., Leibu, R., Newman, H., Rizel, L., Perlman, I., and Ben-Yosef, T. (2015) An intronic deletion in the PROM1 gene leads to autosomal recessive cone-rod dystrophy. Mol. Vis. 21, 1295-1306

16. Jinda, W., Taylor, T. D., Suzuki, Y., Thongnoppakhun, W., Limwongse, C., Lertrit, P., Suriyaphol, P., Trinavarat, A., and Atchaneeyasakul, L. O. (2014) Whole Exome Sequencing in Thai Patients With Retinitis Pigmentosa Reveals Novel Mutations in Six Genes. Invest. Ophth. Vis. Sci. 55, 2259- 2268

17. Zhao, L., Wang, F., Wang, H., Li, Y. M., Alexander, S., Wang, K. Q., Willoughby, C. E., Zaneveld, J. E., Jiang, L. C., Soens, Z. T., Earle, P., Simpson, D., Silvestri, G., and Chen, R. (2015) Nextgeneration sequencing-based molecular diagnosis of 82 retinitis pigmentosa probands from Northern Ireland. Hum. Genet. 134, 217-230

18. Eisenberger, T., Neuhaus, C., Khan, A. O., Decker, C., Preising, M. N., Friedburg, C., Bieg, A., Gliem, M., Issa, P. C., Holz, F. G., Baig, S. M., Hellenbroich, Y., Galvez, A., Platzer, K., Wollnik, B., Laddach, N., Ghaffari, S. R., Rafati, M., Botzenhart, E., Tinschert, S., Borger, D., Bohring, A., Schreml, J., Kortge-Jung, S., Schell-Apacik, C., Bakur, K., Al-Aama, J. Y., Neuhann, T., Herkenrath, P., Nurnberg, G., Nurnburg, P., Davis, J. S., Gal, A., Bergmann, C., Lorenz, B., and Bolz, H. J. (2013) Increasing the Yield in Targeted Next-Generation Sequencing by Implicating CNV Analysis, Non-Coding Exons and the Overall Variant Load: The Example of Retinal Dystrophies. PLoS. One. 8, e78496

19. Permanyer, J., Navarro, R., Friedman, J., Pomares, E., Castro-Navarro, J., Marfany, G., Swaroop, A., and Gonzalez-Duarte, R. (2010) Autosomal Recessive Retinitis Pigmentosa with Early Macular Affectation Caused by Premature Truncation in PROM1. Invest. Ophth. Vis. Sci. 51, 2656-2663

20. Zhang, Q. J., Zulfiqar, F., Xiao, X., Riazuddin, S. A., Ahmad, Z., Caruso, R., MacDonald, I., Sieving, P., Riazuddin, S., and Hejtmancik, J. F. (2007) Severe retinitis pigmentosa mapped to 4p15 and associated with a novel mutation in the PROM1 gene. Hum. Genet. 122, 293-299

21. Han, Z., Anderson, D. W., and Papermaster, D. S. (2012) Prominin-1 localizes to the open rims of outer segment lamellae in Xenopus laevis rod and cone photoreceptors. Invest. Ophthalmol. Vis. Sci. 53, 361-373

22. McGrail, M., Batz, L., Noack, K., Pandey, S., Huang, Y., Gu, X., and Essner, J. J. (2010) Expression of the Zebrafish CD133/prominin1 Genes in Cellular Proliferation Zones in the Embryonic Central Nervous System and Sensory Organs. Dev. Dynam. 239, 1849-1857

23. Stuck, M. W., Conley, S. M., and Naash, M. I. (2016) PRPH2/RDS and ROM-1: Historical context, current views and future considerations. Prog. Retin. Eye. Res. 52, 47-63

24. Zulliger, R., Conley, S. M., Mwoyosvi, M. L., Al-Ubaidi, M. R., and Naash, M. I. (2018) Oligomerization of Prph2 and Rom1 is essential for photoreceptor outer segment formation. Human. Molecular. Genetics. 27, 3507-3518

25. Salles, M. V., Motta, F. L., da Silva, E. D., Teixeira, P. V. L., Costa, K. A., Filippelli-Silva, R., Martin, R., Pesquero, J. B., and Sallum, J. M. F. (2017) PROM1 gene variations in Brazilian patients with macular dystrophy. Ophthalmic. Genetics. 38, 39-42

26. Veleri, S., Lazar, C. H., Chang, B., Sieving, P. A., Banin, E., and Swaroop, A. (2015) Biology and therapy of inherited retinal degenerative disease: insights from mouse models. Dis. Model. Mech. 8, 109-129

27. Crespo, C., and Knust, E. (2018) Characterisation of maturation of photoreceptor cell subtypes during zebrafish retinal development. Biol. Open. 7

28. Kljavin, I. J. (1987) Early development of photoreceptors in the ventral retina of the zebrafish embryo. J. Comp. Neurol. 260, 461-471

29. Raymond, P. A., Barthel, L. K., and Curran, G. A. (1995) Developmental patterning of rod and cone photoreceptors in embryonic zebrafish. J. Comp. Neurol. 359, 537-550

30. Schmitt, E. A., and Dowling, J. E. (1999) Early retinal development in the zebrafish, Danio rerio: light and electron microscopic analyses. J. Comp. Neurol. 404, 515-536

31. Damek-Poprawa, M., Krouse, J., Gretzula, C., and Boesze-Battaglia, K. (2005) A novel tetraspanin fusion protein, peripherin-2, requires a region upstream of the fusion domain for activity. J. Biol. Chem. 280, 9217-9224

32. Sanyal, S., and Jansen, H. G. (1981) Absence of receptor outer segments in the retina of rds mutant mice. Neurosci. Lett. 21, 23-26

33. Jansen, H. G., and Sanyal, S. (1984) Development and degeneration of retina in rds mutant mice: electron microscopy. J. Comp. Neurol. 224, 71-84

34. Boon, C. J., den Hollander, A. I., Hoyng, C. B., Cremers, F. P., Klevering, B. J., and Keunen, J. E. (2008) The spectrum of retinal dystrophies caused by mutations in the peripherin/RDS gene. Prog. Retin. Eye. Res. 27, 213-235

35. Chakraborty, D., Ding, X. Q., Conley, S. M., Fliesler, S. J., and Naash, M. I. (2009) Differential requirements for retinal degeneration slow intermolecular disulfide-linked oligomerization in rods versus cones. Hum. Mol. Genet. 18, 797-808

36. Chakraborty, D., Conley, S. M., Stuck, M. W., and Naash, M. I. (2010) Differences in RDS trafficking, assembly and function in cones versus rods: insights from studies of C150S-RDS. Hum. Mol. Genet. 19, 4799-4812

37. Stuck, M. W., Conley, S. M., and Naash, M. I. (2015) Retinal Degeneration Slow (RDS) Glycosylation Plays a Role in Cone Function and in the Regulation of RDS.ROM-1 Protein Complex Formation. J. Biol. Chem. 290, 27901-27913

38. Chakraborty, D., Ding, X. Q., Fliesler, S. J., and Naash, M. I. (2008) Outer segment oligomerization of Rds: evidence from mouse models and subcellular fractionation. Biochemistry. 47, 1144-1156

39. Lin-Jones, J., Parker, E., Wu, M., Dose, A., and Burnside, B. (2004) Myosin 3A transgene expression produces abnormal actin filament bundles in transgenic Xenopus laevis rod photoreceptors. J. Cell. Sci. 117, 5825-5834

40. Nagle, B. W., Okamoto, C., Taggart, B., and Burnside, B. (1986) The teleost cone cytoskeleton. Localization of actin, microtubules, and intermediate filaments. Invest. Ophthalmol. Vis. Sci. 27, 689-701

41. Sahly, I., Dufour, E., Schietroma, C., Michel, V., Bahloul, A., Perfettini, I., Pepermans, E., Estivalet, A., Carette, D., Aghaie, A., Ebermann, I., Lelli, A., Iribarne, M., Hardelin, J. P., Weil, D., Sahel, J. A., El-Amraoui, A., and Petit, C. (2012) Localization of Usher 1 proteins to the photoreceptor calyceal processes, which are absent from mice. J. Cell. Biol. 199, 381-399

42. Jaszai, J., Fargeas, C. A., Florek, M., Huttner, W. B., and Corbeil, D. (2007) Focus on molecules: prominin-1 (CD133). Exp. Eye. Res. 85, 585-586

43. Conley, S. M., Al-Ubaidi, M. R., Han, Z., and Naash, M. I. (2014) Rim formation is not a prerequisite for distribution of cone photoreceptor outer segment proteins. FASEB. J. 28, 3468- 3479

44. Bhattacharya, S., Yin, J. G., Winborn, C. S., Zhang, Q. H., Yue, J. M., and Chaum, E. (2017) Prominin-1 Is a Novel Regulator of Autophagy in the Human Retinal Pigment Epithelium. Invest. Ophth. Vis. Sci. 58, 2366-2387

45. Zhou, Z., Vinberg, F., Schottler, F., Doggett, T. A., Kefalov, V. J., and Ferguson, T. A. (2015) Autophagy supports color vision. Autophagy. 11, 1821-1832

46. Bergmann, M., Schutt, F., Holz, F. G., and Kopitz, J. (2004) Inhibition of the ATP-driven proton pump in RPE lysosomes by the major lipofuscin fluorophore A2-E may contribute to the pathogenesis of age-related macular degeneration. Faseb. J. 18, 562-564

47. Hu, X. B., Lu, Z. J., Yu, S. S., Reilly, J., Liu, F., Jia, D. N., Qin, Y. Y., Han, S. S., Liu, X. L., Qu, Z., Lv, Y. X., Li, J. Z., Huang, Y. W., Jiang, T., Jia, H. B., Wang, Q., Liu, J. Y., Shu, X. H., Tang, Z. H., and Liu, M. G. (2019) CERKL regulates autophagy via the NAD-dependent deacetylase SIRT1. Autophagy. 15, 453-465

48. Yu, S., Li, C., Biswas, L., Hu, X., Liu, F., Reilly, J., Liu, X., Liu, Y., Huang, Y., Lu, Z., Han, S., Wang, L., Yu Liu, J., Jiang, T., Shu, X., Wong, F., Tang, Z., and Liu, M. (2017) CERKL gene knockout disturbs photoreceptor outer segment phagocytosis and causes rod-cone dystrophy in zebrafish. Hum. Mol. Genet. 26, 2335-2345

49. Liu, F., Qin, Y., Yu, S., Soares, D. C., Yang, L., Weng, J., Li, C., Gao, M., Lu, Z., Hu, X., Liu, X., Jiang, T., Liu, J. Y., Shu, X., Tang, Z., and Liu, M. (2017) Pathogenic mutations in retinitis pigmentosa 2 predominantly result in loss of RP2 protein stability in humans and zebrafish. J. Biol. Chem. 292, 6225-6239

50. Lu, Z. J., Hu, X. B., Liu, F., Soares, D. C., Liu, X. L., Yu, S. S., Gao, M., Han, S. S., Qin, Y. Y., Li, C., Jiang, T., Luo, D. J., Guo, A. Y., Tang, Z. H., and Liu, M. G. (2017) Ablation of EYS in zebrafish causes mislocalisation of outer segment proteins, F-actin disruption and cone-rod dystrophy. Sci. Rep. 7, 46098

Footnotes

This work was supported by grants from the National Natural Science Foundation of China (No. 81800870, 31571303, 31801041, 81670890 and 31871260).

Abbreviations: TELAN, transcription activator-like effector nucleases; OS, outer-segment; ONL, outer nuclear layer; INL, inner nuclear layer; RPE, retinal pigment epithelium; TEM, Transmission electron microscopy; WT, wild type; MT, mutant type.

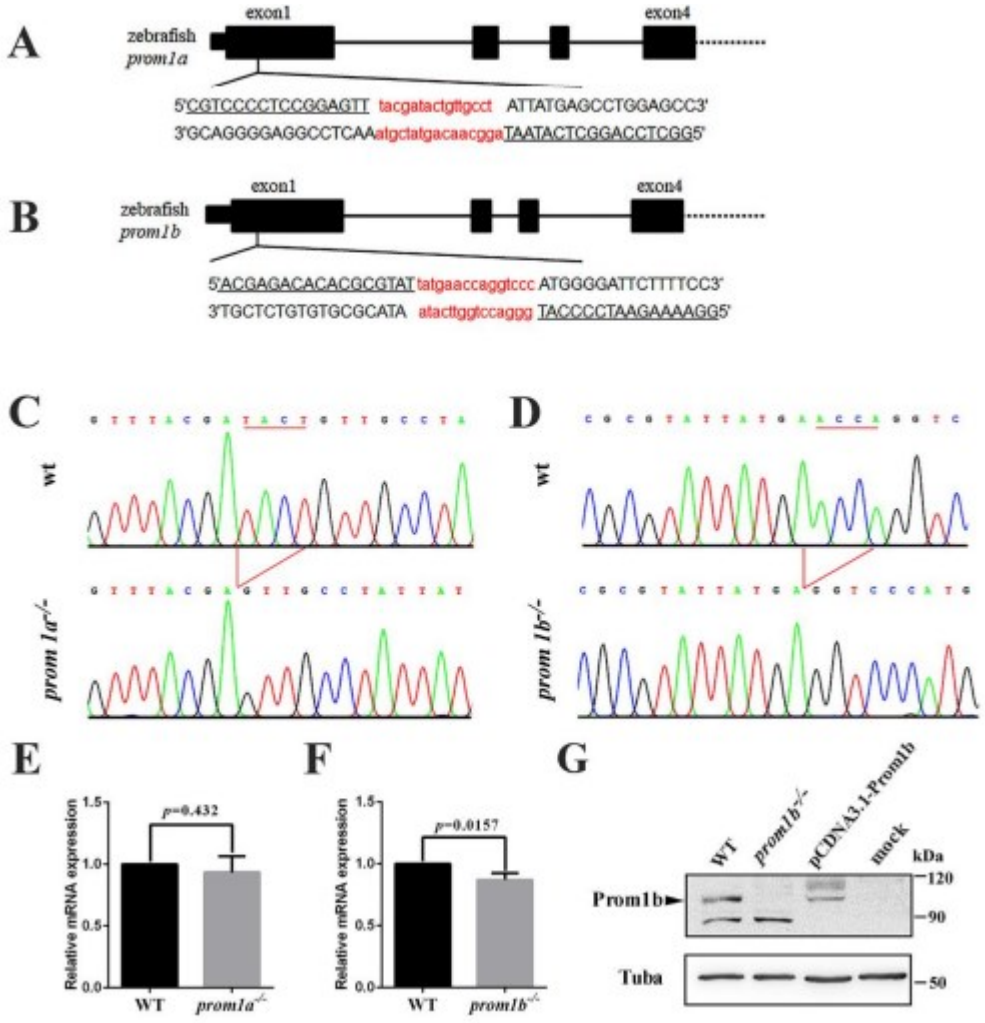

Figure 1. Generation of the prom1a$^{-/-}$ and prom1b$^{-/-}$ zebrafish lines**.** (A and B) Zebrafish prom1a and prom1b gene are shown with the left and right arms of the TALE binding sequences underlined, and the spacer sequences highlighted in red. C. Sequencing of the c.138_141delTACT prom1a mutation in homozygous zebrafish. The 4-bp deletion is indicated by the red line. D. Sequencing of the c.174_177delACCA prom1b mutation in homozygous zebrafish. The 4-bp deletion is indicated by the red line. (E and F) Quantitative real-time PCR analysis of prom1a at 2mpf and prom1b at 7dpf. gapdh served as endogenous control. Means ± SD of 3 repeats are shown. (G) Western blot analysis of Prom1b in retinal extracts from WT and prom1b-/- zebrafish at 1mpf. The zebrafish pCDNA3.1-Prom1b expressed in HLECs was used as a positive control, and the mock as a negative control. Tuba served as a loading control. The Prom1b band marked by the black arrowhead is undetectable in prom1b$^{-/-}$ zebrafish.

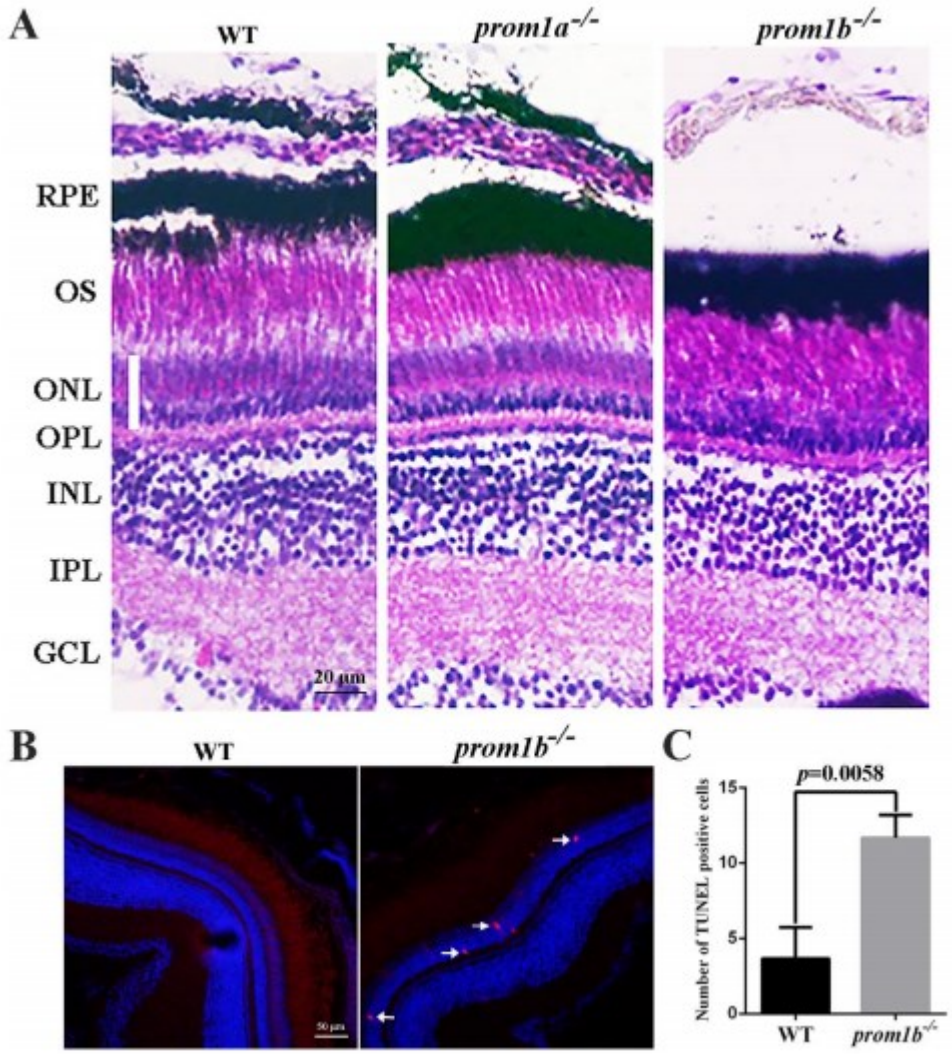

Figure 2. prom1b$^{-/-}$ zebrafish displayed retinal degeneration phenotypes**.** (A) Retinal histology analysis of WT and prom1a/1b-knockout zebrafish at 1mpf. RPE, retinal pigment epithelium; OS, outer-segment; IS, inner segment; ONL, outer nuclear layer; OPL, outer plexiform layer; INL, inner nuclear layer; IPL, inner plexiform layer; GCL, ganglion cell layer. Scale bars, 20 μm. (B) TUNEL staining of WT and prom1b$^{-/-}$ zebrafish at 1mpf. White arrows indicate the TUNEL positive signals (red). Scale bars, 50 μm. (C) Quantification of TUNEL positive cells in ONL of whole-retina sections at 1mpf (n=3).

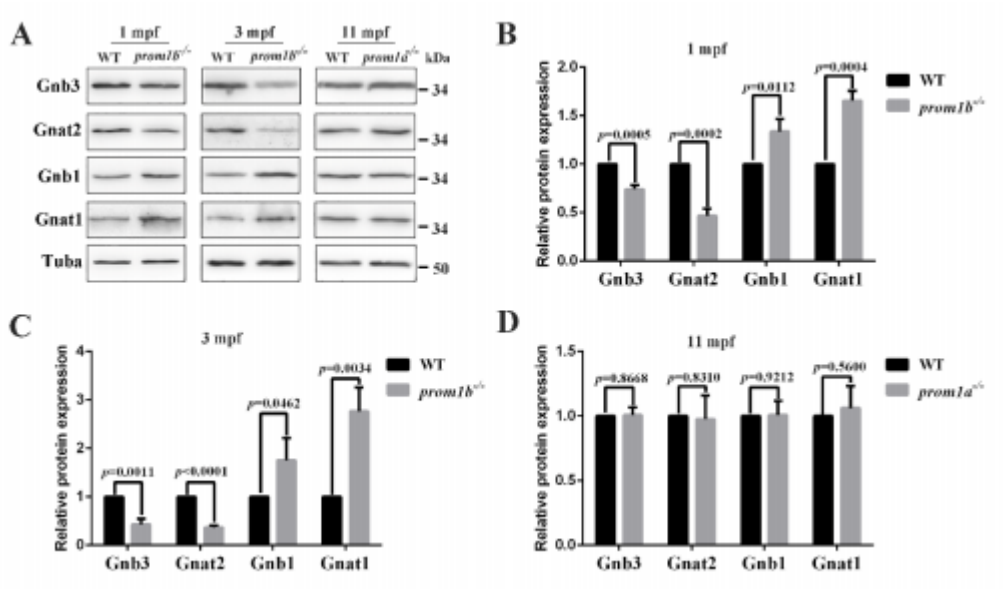

Figure 3. Expression of phototransduction cascade proteins was affected in prom1b$^{-/-}$ zebrafish. (A) Protein levels of Gnb3, gnat2, Gnb1 and Gnat1 were detected by western blot in WT and prom1a/1bknockout zebrafish at indicated ages. Gnb3 and Gnat2 express specifically in cones, while Gnb1 and Gnat1 express specifically in rods. Tuba was used as an endogenous control. (B, C and D) Relative levels of proteins presented in panels A. Means ±SD of 3 repeats are shown.

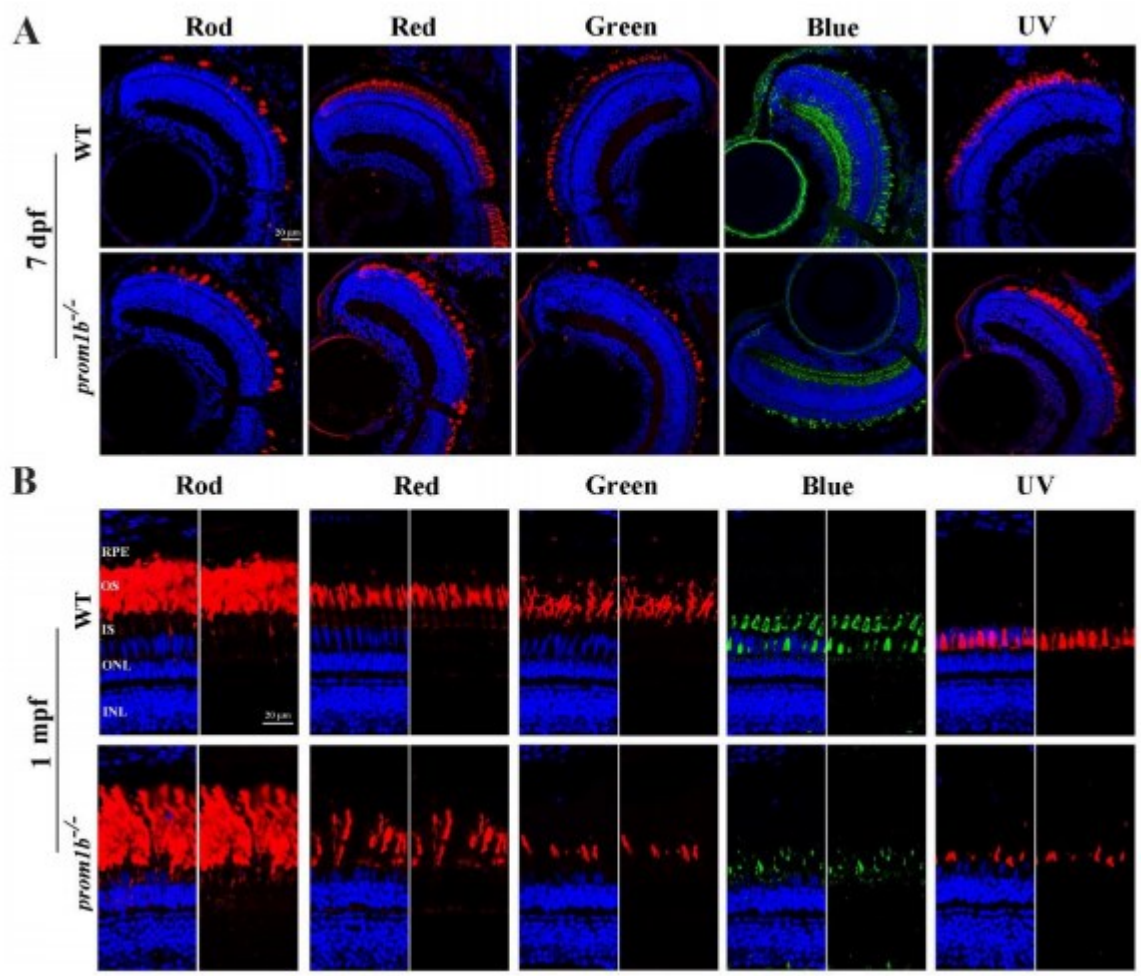

Figure 4. Prom1b deletion in zebrafish caused different impairment in different photoreceptor types. (A and B) Retinal cryosections from WT and prom1b$^{-/-}$ zebrafish showing rods and cones at 7dpf and 1mpf by immunofluorescence stain. Rods are labelled with anti-Rhodopsin antibody (red); red cones are labelled with anti-Opn1lw antibody (red); green cones are labelled with anti-Opn1mw antibody (red); blue cones are labelled with anti-Opn1sw2 antibody (green); UV cones are labelled with anti-Opn1sw1 antibody (red); nuclei are labelled with DAPI (blue). Scale bars, 20 μm.

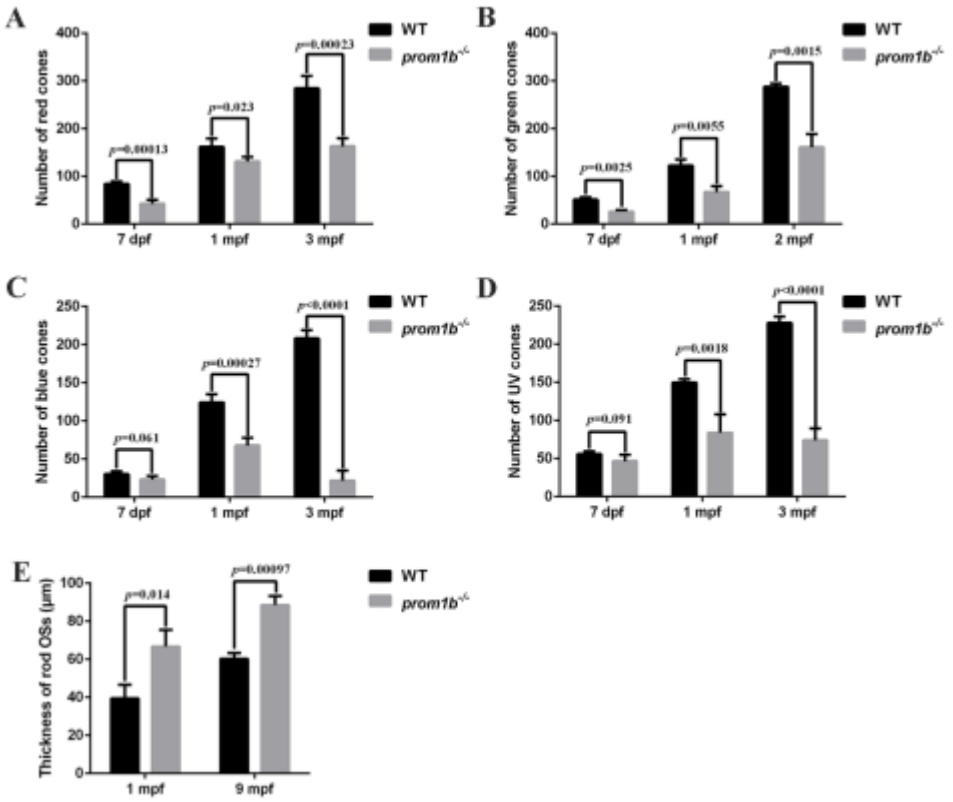

Figure 5. Statistical data for rods and cones at indicated ages. (A) Quantification of red cones in wholeretina sections of WT and prom1b$^{-/-}$ zebrafish (n=4). (B) Quantification of green cones in whole-retina sections of WT and prom1b$^{-/-}$ zebrafish (n=3). (C) Quantification of blue cones in whole-retina sections of WT and prom1b$^{-/-}$ zebrafish (n=4). (D) Quantification of UV cones in whole-retina sections of WT and prom1b$^{-/-}$ zebrafish (n=4). (E) The thickness of rod OSs was counted versus distance (100 μm) from the optic nerve head (n=3).

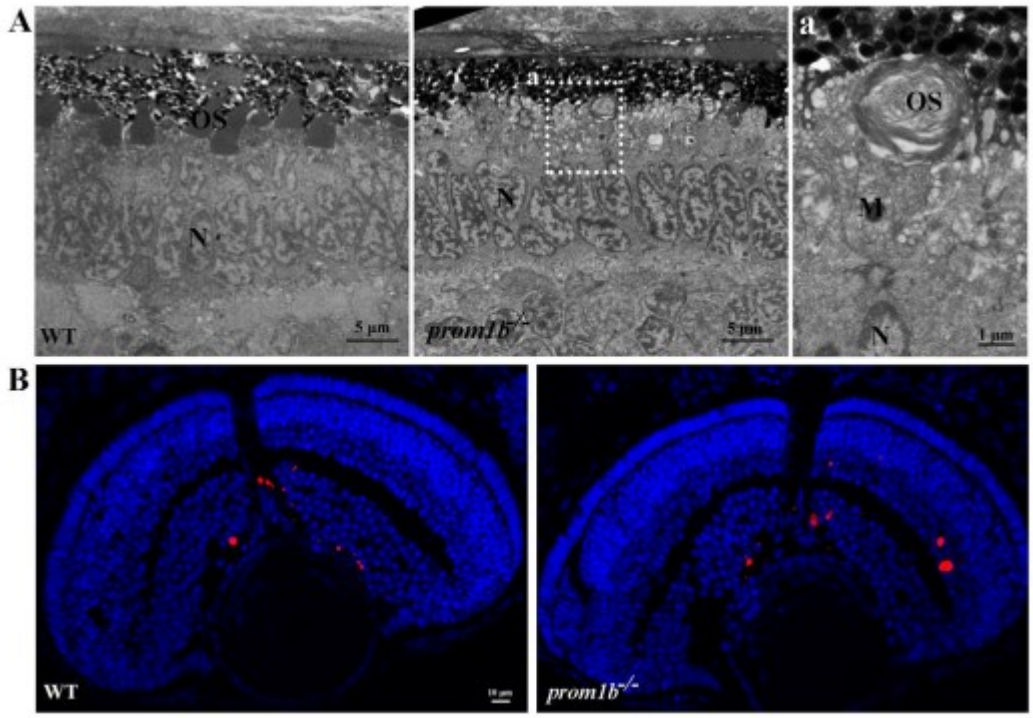

Figure 6. Morphogenesis of OSs was delayed in prom1b$^{-/-}$ zebrafish at 3dpf. (A) Ultrastructural analysis of WT and prom1b$^{-/-}$ zebrafish photoreceptors at 3dpf. WT zebrafish retina showed well-stacked outersegments, while there were few disk structures detected in prom1b$^{-/-}$ zebrafish. The area within the dotted rectangles (a) is shown in the higher magnification image on the right. N, nuclei; M, mitochondria; OS, outer-segment. Scale bars, 5 μm. (B) TUNEL staining showed no differences in cell death in the ONL of prom1b$^{-/-}$ and WT zebrafish at 3dpf. The signal of apoptotic positive cells is red. Scale bars, 10 μm.

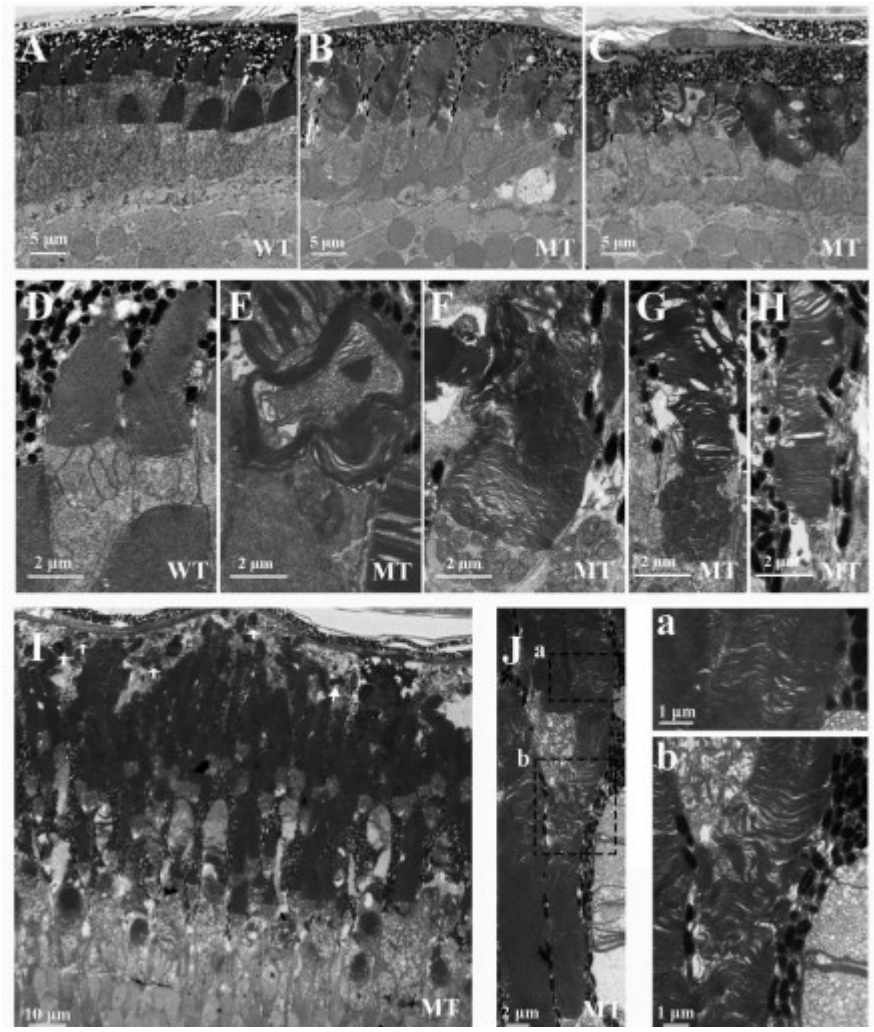

Figure 7. Outer-segment morphogenesis was disrupted in prom1b$^{-/-}$ zebrafish (A-C) Ultrastructural analysis of WT and MT (prom1b$^{-/-}$) zebrafish photoreceptors at 10dpf. Scale bars, 5 μm. (D-H) Outersegment disks of MT zebrafish exhibited different morphological characteristics compared with WT zebrafish. Scale bars, 2 μm. (I and J) Retinal ultrastructural analysis of MT zebrafish photoreceptors at 2mpf. White arrows indicate the shedding OSs. The areas within the dashed rectangles are shown in the higher magnification images (a, b). Scale bars: 10 μm in (I); 2 μm in (J); 1 μm in (a, b).

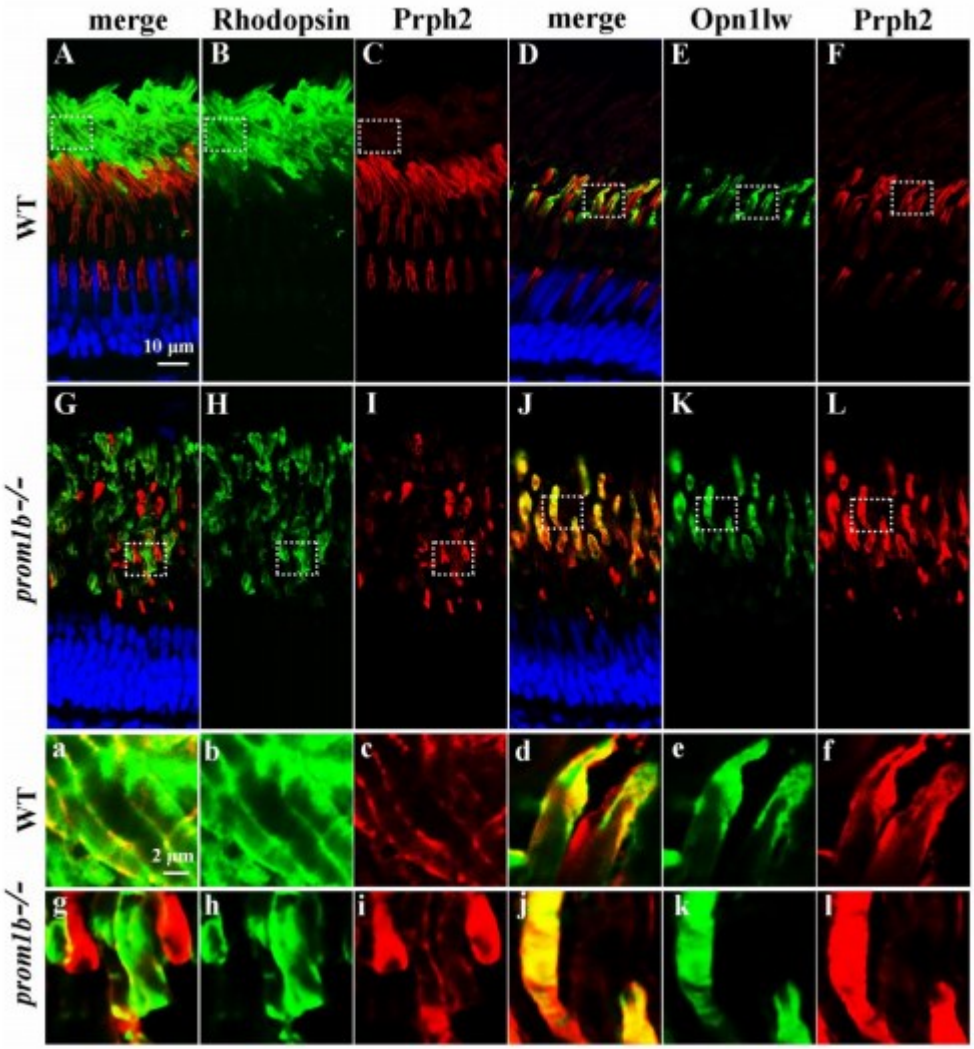

Figure 8. Prph2 were mislocalized in prom1b$^{-/-}$ zebrafish. (A-C, G-I) Retinal cryosections from WT and prom1b$^{-/-}$ zebrafish were immunostained with anti-Rhodopsin (green) and anti-Prph2 (red) antibodies at 2mpf. Occasionally mislocalization of Prph2 appeared in the partial OSs of rods. The areas within the dashed rectangles are shown in the higher magnification images (a-c, g-i). Scale bars: 10 μm in (A-C, G-I); 2 μm in (a-c, g-i). (D-F, J-L) Retinal cryosections from WT and prom1b-/- zebrafish were immunostained with anti-opn1LW (green) and anti-Prph2 (red) antibodies at 2mpf. The OS of red cones in prom1b-/- zebrafish showed mislocalization of Prph2.The areas within the dashed rectangles are shown in the higher magnification images (d-f, j-i). Scale bars: 10 μm in (D-F, J-L); 2 μm in (d-f, j-l).

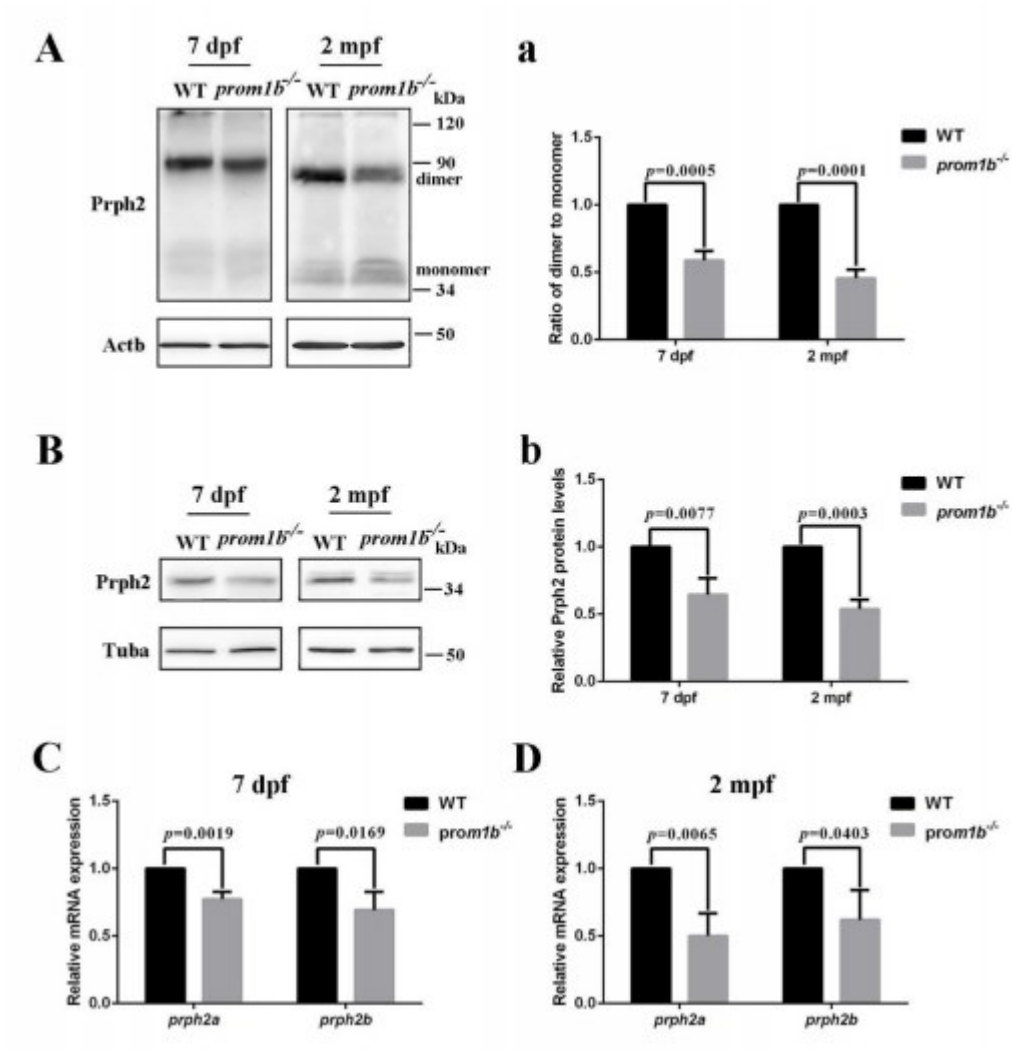

Figure 9. Prom1b deletion affects Prph2 protein expression and oligomerization. (A) Non-reducing Western blot analysis of Prph2 in retinal extracts from WT and prom1b-/- zebrafish at indicated ages. Actb was used as an endogenous control. (B) Western blot analysis of Prph2 in retinal extracts from WT and prom1b-/- zebrafish at indicated ages. Tuba was used as an endogenous control. (C and D) Quantitative realtime PCR analysis of prph2a and prph2b in WT and prom1b-/- zebrafish at indicated ages. Gapdh served as endogenous control. Means ± SD of 3 repeats are shown. (a and b) Relative levels of proteins presented in panels A and B. Means ± SD of 3 repeats are shown.